

## $\text{Ni}_{56}\text{Mn}_{25-x}\text{Cr}_x\text{Ga}_{19}$ ( $x=0, 2, 4, 6$ ) high temperature shape memory alloys

MA Yun-qing, LAI San-li, YANG Shui-yuan, LUO Yu, WANG Cui-ping, LIU Xing-jun

College of Materials, Xiamen University, Xiamen 361005, China

Received 21 January 2010; accepted 10 May 2010

**Abstract:** The microstructure, martensitic transformation behavior, mechanical and shape memory properties of  $\text{Ni}_{56}\text{Mn}_{25-x}\text{Cr}_x\text{Ga}_{19}$  ( $x=0, 2, 4, 6$ ) alloys were investigated. Single phase of martensite with tetragonal structure is present for  $x=0$ , and dual-phase containing martensite and  $\gamma$  phase is observed for  $x \geq 2$ . The martensitic transformation peak temperatures decrease monotonically from 401 °C for  $x=0$  to 197 °C for  $x=6$ . The introduction of  $\gamma$  phase by Cr addition is proved to be effective in improving the workability and ductility. The tensile stress and strain are 497 MPa and 8 % for  $x=4$ , and 454 MPa and 5.5 % for  $x=6$ , respectively. The shape memory strain values are 2.7 % under a residual strain of 4.5 % for  $x=4$ , and 1.9 % under a residual strain of 3.5 % for  $x=6$ , respectively.

**Key words:** martensitic transformation; tension; ductility; high-temperature shape-memory effect

### 1 Introduction

In the last decade, the Heusler Ni-Mn-Ga alloy has attracted much attention due to its large magnetic field induced strain and high response frequency[1–3]. Meanwhile, several papers revealed that a high martensitic transformation temperature (up to 350 °C) exists in Ni-Mn-Ga alloys with Ni content higher than the stoichiometric  $\text{Ni}_2\text{MnGa}$ [4–5], showing their potentials as high-temperature shape-memory alloys (HTSMAs). Subsequent investigations revealed a variety of excellent properties in single-crystalline  $\text{Ni}_{56}\text{Mn}_{25}\text{Ga}_{19}$ , including a martensitic transformation temperature higher than 250 °C, excellent thermal stability[6], and over 6% shape-memory effect (SME)[7–8]. All these have made Ni-Mn-Ga alloys be promising HTSMAs. However, Ni-Mn-Ga alloys are extremely brittle in the polycrystalline state. Therefore, the studies on improving their workability and ductility keep active.

As a matter of fact, introducing the ductile  $\gamma$  phase is an effective method for the ductility enhancement of B2-type intermetallic compounds, such as Fe doped Ni-Al SMA[9] and  $\beta+\gamma$  two-phase in Co-Ni-Al SMA[10]. Similarly, in order to improve the ductility of Ni-Mn-Ga alloys, there has also been growing interest in adding the

fourth element, such as Fe, Co, Cu, Ti or rare elements, to form a ductile second phase[11–14]. And the improvement of the ductility and mechanical properties has been successfully achieved by introducing sufficient amount of ductile  $\gamma$  phase or refinement of grain size. Up to today, little information about the addition of Cr into Ni-Mn-Ga alloys has been reported. Therefore, the purpose of this work is to investigate the effect of Cr addition on the microstructure, martensitic transformation behavior, as well as the mechanical and shape memory properties of  $\text{Ni}_{25}\text{Mn}_{25-x}\text{Cr}_x\text{Ga}_{19}$  ( $x=0, 2, 4, 6$ ) alloys.

### 2 Experimental

Polycrystalline buttons of  $\text{Ni}_{25}\text{Mn}_{25-x}\text{Cr}_x\text{Ga}_{19}$  ( $x=2, 4, 6$ ) alloys were arc-melted five times under argon atmosphere to ensure uniformity. The purities of the nickel, manganese, gallium and chromium were 99.9%, 99.7%, 99.99% and 99.9%, respectively. The metal buttons were sealed into vacuum quartz ampoules and annealed at 900 °C for 72 h. Then the buttons were heated to 900 °C and conducted to hot rolling. During the hot rolling, some little cracks were generated. However, hot rolling could be continued after cleaning these cracks. Finally, the button ingots were successfully

**Foundation item:** Project(50771086) supported by the National Natural Science Foundation of China; Project(NCET-09-0676) supported by Program for New Century Excellent Talents in University (NCET), China; Project supported by Program for New Century Excellent Talents in Fujian Provincial University (NCETFJ), China; Project(2009H0039) supported by Fujian Provincial Department of Science and Technology, China

**Corresponding author:** MA Yun-qing; Tel: +86-592-2189688; Fax: +86-592-2187966; E-mail: [myq@xmu.edu.cn](mailto:myq@xmu.edu.cn)  
DOI: 10.1016/S1003-6326(11)60683-3

hot rolled to thin plates with 1 mm in thickness.

The phase structure was identified at room temperature on a Panalytical X'pert PRO with Cu  $K_{\alpha}$  radiation. The microstructure was observed by optical microscope. Samples for optical observation were mechanically polished and etched in a solution of 99 mL methanol +2 mL nitric acid +5 g ferric chloride. The martensitic transformation temperatures were determined on a differential scanning calorimeter (DSC) (Netzsch STA 404) at heating and cooling rates of 10 °C/min. The chemical compositions of martensite phases and  $\gamma$  phases were obtained on an electron probe microanalyzer (JEOL, JXA-8100). The mechanical properties and SME were measured by tensile tests at ambient temperature using a Galdabini Sun 2500 machine at a crosshead speed of 0.2 mm/min. Details of tensile tests for the mechanical properties and SME are identical to our previous study[14].

### 3 Results and discussion

#### 3.1 Microstructure

Fig.1 shows the XRD patterns of  $Ni_{56}Mn_{25-x}Cr_xGa_{19}$  ( $x=0, 2, 4, 6$ ) alloys at room temperature. When  $x=0$ , all reflection peaks can be indexed with the tetragonal-structure martensite (denoted as M), with main diffraction peaks of (111), (400), (004), (440), (044), (622) and (444). When  $x \geq 2$ , in addition to the seven diffraction peaks from martensite phase, three additional peaks appear, as indicated by arrows in Fig.1. The new phase is confirmed as a face-centered cubic (fcc)  $\gamma$  phase (denoted as  $\gamma$ ) with main diffraction peaks of (111), (200), (202), (311) and (222). The  $\gamma(111)$  and  $\gamma(222)$  diffraction peaks overlap with the M(222) and M(444) peaks, respectively. Meanwhile, it is worth noting that the intensities of the diffraction peaks of  $\gamma$  phase increase with increasing Cr content, implying the increase of the amount of  $\gamma$  phase. The crystal lattice parameters of martensite phase are calculated and listed

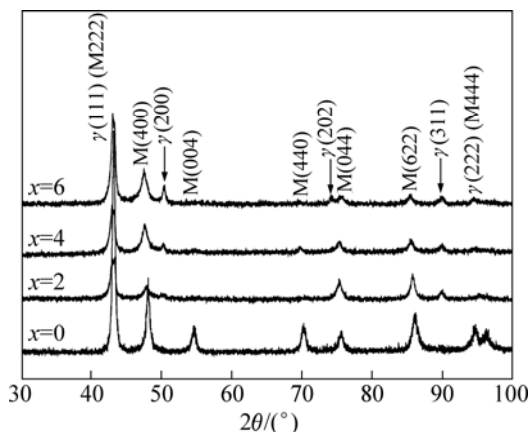


Fig.1 XRD patterns of  $Ni_{56}Mn_{25-x}Cr_xGa_{19}$  ( $x=0, 2, 4, 6$ ) alloys

**Table 1** Lattice parameters and crystal volumes of martensite phase in  $Ni_{56}Mn_{25-x}Cr_xGa_{19}$  ( $x=0, 2, 4, 6$ ) alloys

Composite	Lattice parameter/Å		$c/a$	Unit cell volume/Å <sup>3</sup>
	$a$	$c$		
$Ni_{56}Mn_{25}Ga_{19}$	7.552	6.706	0.888	382.5
$Ni_{56}Mn_{23}Cr_2Ga_{19}$	7.623	6.597	0.865	383.4
$Ni_{56}Mn_{21}Cr_4Ga_{19}$	7.628	6.622	0.868	385.3
$Ni_{56}Mn_{19}Cr_6Ga_{19}$	7.642	6.613	0.865	386.2

in Table 1. It could be seen that the unit-cell volumes of martensite phase increase gradually with increasing Cr content. However, the lattice parameter of the  $\gamma$  phase remains almost constant,  $a=3.614$  Å.

Fig.2 shows the optical microstructures of  $Ni_{56}Mn_{25-x}Cr_xGa_{19}$  ( $x=0, 2, 4, 6$ ) alloys at room temperature. The single martensite phase structure could be obviously observed when  $x=0$ , identical to that in the single phase of  $Ni_{54}Mn_{25}Ga_{21}$  alloy[15], as shown in Fig.2(a). Whereas, two phase structures are present with Cr addition, including a grey matrix and a white second phase, as shown in Figs.2(b)–(d). The grey phase is martensite phase with typically lamellar morphology; and the white phase is confirmed to be a fcc structured  $\gamma$  phase according to the XRD patterns and the previous investigations[14–15]. The  $\gamma$  phase dispersed uniformly among the martensite variants and the grain boundaries, and their amounts increased with increasing Cr content. The volume fractions of the  $\gamma$  phase were measured to be about 10%, 16% and 21% for  $x=2, 4$  and 6, respectively. It is worth noting that the shape and the configuration of  $\gamma$  phase have obvious change when  $x=6$ , where some of the  $\gamma$  phases join together to form slender bars, as shown in Fig.2(d). These varieties may have important effects on the mechanical and shape memory properties of  $Ni_{56}Mn_{25-x}Cr_xGa_{19}$  ( $x=0, 2, 4, 6$ ) alloys.

#### 3.2 Martensitic transformation behavior

Fig.3 shows a typical DSC results of  $Ni_{56}Mn_{21}Cr_4Ga_{19}$  alloys. The martensitic transformations are reversible. The starting temperature for austenite transformation  $A_s$ , the peak temperature  $A_p$  and the finishing temperature  $A_f$  are 344 °C, 355 °C and 377 °C, respectively. The martensitic starting temperature  $M_s$ , the peak temperature  $M_p$  and the finishing temperature  $M_f$  are 270, 258 and 238 °C. The hysteresis temperature is about 97 °C, which is taken as the difference between the peak temperatures of austenite transformation and martensitic transformation. In the same way, the transformation temperatures are determined for all the  $Ni_{56}Mn_{25-x}Cr_xGa_{19}$  ( $x=0, 2, 4, 6$ ) alloys and are summarized in Table 2. It can be seen that the martensitic transformation temperatures gradually

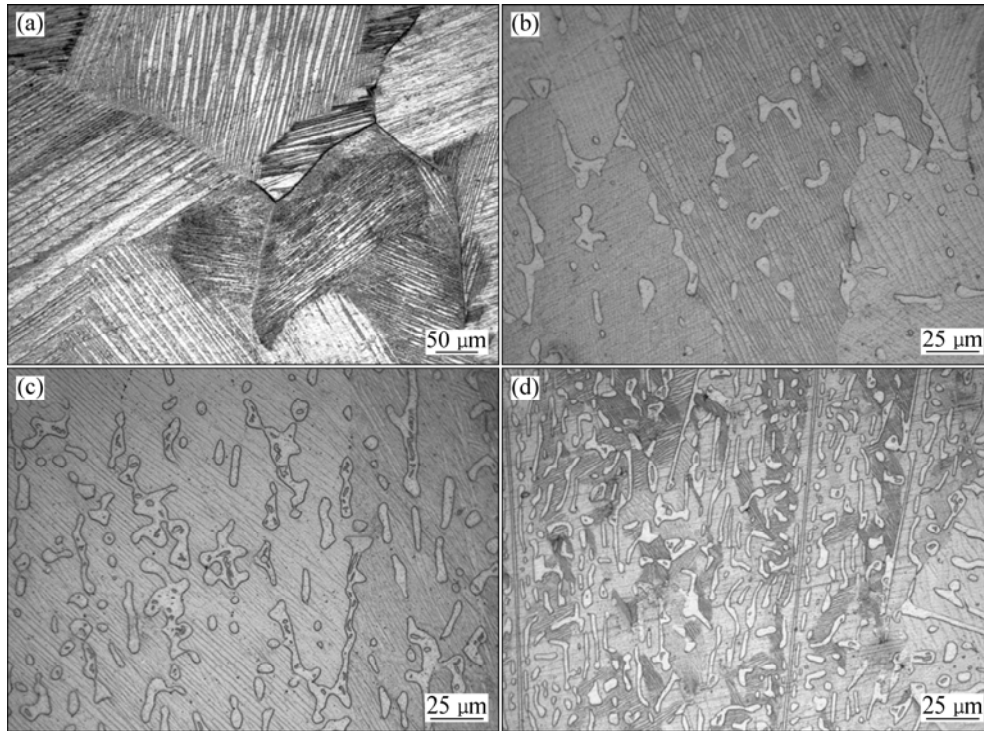


**Fig.2** Optical microstructures of  $\text{Ni}_{56}\text{Mn}_{25-x}\text{Cr}_x\text{Ga}_{19}$  alloys: (a)  $x=0$ ; (b)  $x=2$ ; (c)  $x=4$ ; (d)  $x=6$

**Table 2** Austenite and martensitic transformation temperature of  $\text{Ni}_{56}\text{Mn}_{25-x}\text{Cr}_x\text{Ga}_{19}$  ( $x=0, 2, 4, 6$ ) alloys

Composite	$A_s/^\circ\text{C}$	$A_p/^\circ\text{C}$	$A_f/^\circ\text{C}$	$M_s/^\circ\text{C}$	$M_p/^\circ\text{C}$	$M_f/^\circ\text{C}$	Hysteresis temperature/ $^\circ\text{C}$
$\text{Ni}_{56}\text{Mn}_{21}\text{Ga}_{19}$	441	452	463	403	401	393	51
$\text{Ni}_{56}\text{Mn}_{23}\text{Cr}_2\text{Ga}_{19}$	408	427	452	367	354	330	73
$\text{Ni}_{56}\text{Mn}_{21}\text{Cr}_4\text{Ga}_{19}$	344	355	377	270	258	238	97
$\text{Ni}_{56}\text{Mn}_{19}\text{Cr}_6\text{Ga}_{19}$	289	303	315	220	197	181	106

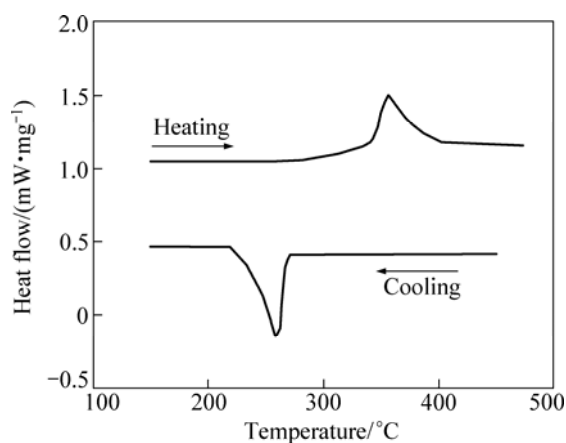


**Fig.3** Typical DSC results of  $\text{Ni}_{56}\text{Mn}_{21}\text{Cr}_4\text{Ga}_{19}$  alloys showing forward (on cooling) and reverse (on heating) martensitic transformation

decrease with increasing Cr content, where the peak temperature is from  $401^\circ\text{C}$  for  $x=0$  to  $197^\circ\text{C}$  for  $x=6$ , and the corresponding hysteresis temperature increases from  $51^\circ\text{C}$  to  $106^\circ\text{C}$ . However, both  $M_s$  and  $A_s$

temperatures are still above  $200^\circ\text{C}$  as long as the Cr content does not exceed 6%. All these suggest  $\text{Ni}_{56}\text{Mn}_{25-x}\text{Cr}_x\text{Ga}_{19}$  alloys being promising HTSMAs.

The chemical compositions of the martensite phase of  $\text{Ni}_{56}\text{Mn}_{25-x}\text{Cr}_x\text{Ga}_{19}$  ( $x=0, 2, 4, 6$ ) alloys are measured and summarized in Table 3, and the electron concentration ( $e/a$ ) is calculated by the following equation:

$$e/a = x_{\text{Ni}}e^{\text{Ni}} + x_{\text{Mn}}e^{\text{Mn}} + x_{\text{Cr}}e^{\text{Cr}} + x_{\text{Ga}}e^{\text{Ga}}$$

where  $x_{\text{Ni}}$ ,  $x_{\text{Mn}}$ ,  $x_{\text{Cr}}$  and  $x_{\text{Ga}}$  represent the mole fractions of elements; and  $e^{\text{Ni}}$ ,  $e^{\text{Mn}}$ ,  $e^{\text{Cr}}$  and  $e^{\text{Ga}}$  represent the corresponding number of valence electrons, which are 10, 7, 6 and 3, respectively. For the partial substitution of Mn by Cr, the martensitic transformation temperatures decrease with increasing Cr content. This is likely to be resulted from the variation in the intrinsic factors, i.e. the increase in the unit-cell volume and the decrease in the electron concentration ( $e/a$ ) with increasing Cr content because Cr possesses larger atomic radius and lower electron concentration compared with Mn. These results are consistent with the previous investigations[16–18].

Moreover, it is supposed to be feasible that further adding some elements with high electron concentration, such as Ni, Cu, will be helpful to keep the high martensitic transformations of Ni-Mn-Cr-Ga alloys[13, 15, 19].

**Table 3** Chemical compositions and electron concentrations (*e/a*) of martensite phase in Ni<sub>56</sub>Mn<sub>25-x</sub>Cr<sub>x</sub>Ga<sub>19</sub> (*x*=0, 2, 4, 6) alloys

Nominal composite	<i>x</i> /%				<i>e/a</i>
	Ni	Mn	Cr	Ga	
Ni <sub>56</sub> Mn <sub>21</sub> Ga <sub>19</sub>	55.57	27.03	–	17.39	7.97
Ni <sub>56</sub> Mn <sub>23</sub> Cr <sub>2</sub> Ga <sub>19</sub>	56.55	25.01	1.49	16.95	8.00
Ni <sub>56</sub> Mn <sub>21</sub> Cr <sub>4</sub> Ga <sub>19</sub>	55.31	24.14	2.60	17.96	7.92
Ni <sub>56</sub> Mn <sub>19</sub> Cr <sub>6</sub> Ga <sub>19</sub>	54.69	23.04	3.49	18.78	7.85

**3.3 Mechanical and shape memory properties**

In order to investigate the workability of Ni<sub>56</sub>Mn<sub>25-x</sub>Cr<sub>x</sub>Ga<sub>19</sub> (*x*=0, 2, 4, 6) alloys, hot rolling was attempted for all experimental alloys. When *x*≤2, the buttons cracked seriously due to the insufficient amount of ductile  $\gamma$  phase. When *x*≥4, the buttons could be hot rolled into thin plates of 1 mm in thickness with smooth surface and regular edges, implying that the hot workability and ductility of Ni-Mn-Ga alloys were greatly improved by Cr addition. Their mechanical properties and SMEs were measured by tensile tests. The results are illustrated in Fig.4. The symbol (×) represents the fracture point, and the tensile stress and strain were measured to be 497 MPa and 8% for *x*=4, and 454 MPa and 5.5% (7.5%–2.0%) for *x*=6, respectively. The yield strengths ( $\sigma_s$ ) are 217 MPa and 121 MPa for *x*=4 and *x*=6, respectively, as shown in Fig.4. With a more amount of  $\gamma$  phases through Cr addition,  $\sigma_s$  decreases, implying that the  $\gamma$  phase is soft. According to our previous investigations on the deformation and fracture mechanism of Ni-Mn-Co-Ga alloys by in-situ SEM observation during tensile test[14], the present situation

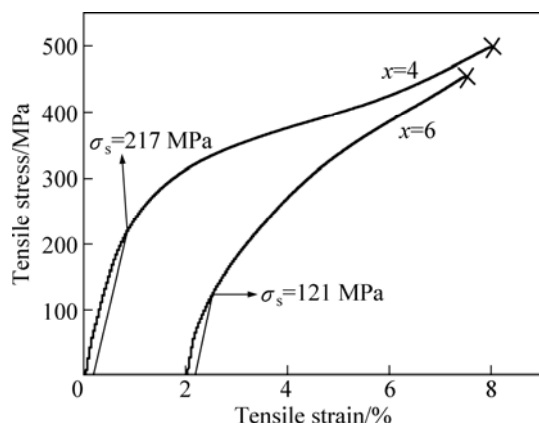


**Fig.4** Tensile stress—strain curves of Ni<sub>56</sub>Mn<sub>25-x</sub>Cr<sub>x</sub>Ga<sub>19</sub> (*x*=4, 6) plates obtained at room temperature

for Ni-Mn-Cr-Ga alloys is almost the same. The yield of the specimen is mostly provided by the deformation of  $\gamma$  phase, coexisting with the reorientations of martensitic variants. However, the tensile elongation of Ni<sub>56</sub>Mn<sub>19</sub>Cr<sub>6</sub>Ga<sub>19</sub> is lower than that of Ni<sub>56</sub>Mn<sub>21</sub>Cr<sub>4</sub>Ga<sub>19</sub>, even though the former contains more ductile  $\gamma$  phase, as obtained from optical observation. The reasons are still unclear now. More investigations are needed on this issue.

In order to investigate the SMEs of the Ni-Mn-Cr-Ga alloys, the specimens were tensioned to different pre-strains. Fig.5(a) shows the stress—strain curve at pre-strain of 5.5 % for Ni<sub>56</sub>Mn<sub>21</sub>Cr<sub>4</sub>Ga<sub>19</sub> alloy. The residual strain after unloading is 4.5%. The arrowed line represents the recovery strain after heating to 500 °C. The recoverable strain is 2.7% and the recoverable rate is 60%. Similarly, Ni<sub>56</sub>Mn<sub>19</sub>Cr<sub>6</sub>Ga<sub>19</sub> alloy exhibits recoverable strain of 1.9 %, and recoverable rate of 54% at the residual strain of 3.5% (The pre-strain is 4.2%), as shown in Fig.5(b). Fig.6 shows the recovery strains at different residual strains for Ni<sub>56</sub>Mn<sub>21</sub>Cr<sub>4</sub>Ga<sub>19</sub> and Ni<sub>56</sub>Mn<sub>19</sub>Cr<sub>6</sub>Ga<sub>19</sub> alloys. It can be seen that the recovery strains increase gradually with increasing residual strains in both alloys. The SME of Ni<sub>56</sub>Mn<sub>19</sub>Cr<sub>6</sub>Ga<sub>19</sub> is lower

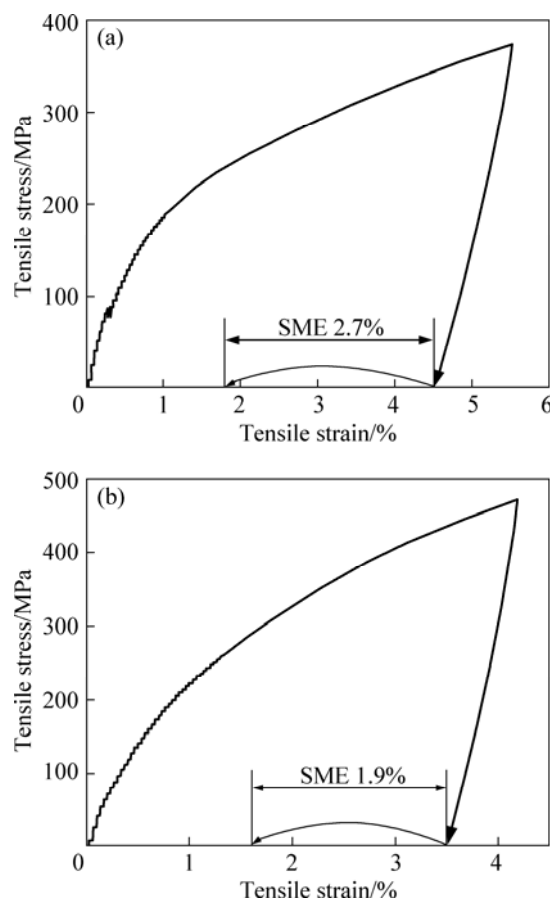


**Fig.5** SME curves of Ni<sub>56</sub>Mn<sub>21</sub>Cr<sub>4</sub>Ga<sub>19</sub> alloy at pre-strain of 5.5% (a) and Ni<sub>56</sub>Mn<sub>19</sub>Cr<sub>6</sub>Ga<sub>19</sub> alloy at pre-strain of 4.2% (b) (The arrow represents strain recovery after heating to 500 °C)

than that of  $\text{Ni}_{56}\text{Mn}_{21}\text{Cr}_4\text{Ga}_{19}$ . This should be understandable if we remember that the yield stress of  $\text{Ni}_{56}\text{Mn}_{19}\text{Cr}_6\text{Ga}_{19}$  is much lower than that of  $\text{Ni}_{56}\text{Mn}_{21}\text{Cr}_4\text{Ga}_{19}$ . Low yield strength will bring about more nonreversible plastic deformation, which is harmful to SME.

Compared with single crystalline  $\text{Ni}_{54}\text{Mn}_{25}\text{Ga}_{21}$  alloy[15], Ni-Mn-Cr-Ga alloys exhibit poor SME. This can be understood by considering the structural reasons. One important item is the existence of the  $\gamma$  phase in Ni-Mn-Cr-Ga alloys. It has been demonstrated that in dual-phase Ni-Al-Fe alloys that the pseudoelastic strain recovery and shape memory recovery strain degraded with increasing volume fraction of  $\gamma$  phase. Similarly, it is believed that the reorientation of martensitic variants and/or detwinning is hampered by  $\gamma$  phase particles dispersed in martensitic matrix[11], and  $\gamma$  phase is also barrier to the shape recovery to the parent phase of the Ni-Mn-Cr-Ga alloys from deformed martensite. In addition, the existence of the grain boundaries in the polycrystalline Ni-Mn-Cr-Ga alloys may also result in the decrease of SME, compared with single crystalline  $\text{Ni}_{54}\text{Mn}_{25}\text{Ga}_{21}$  alloy.

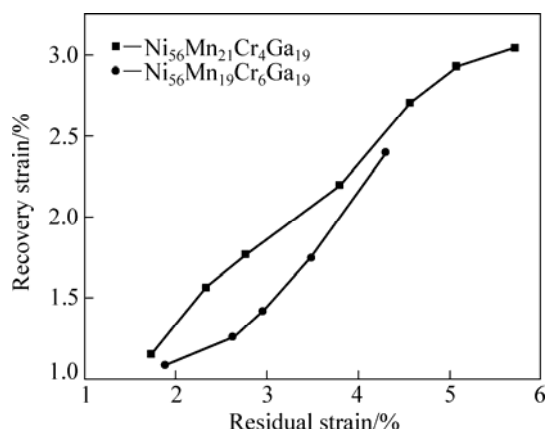


Fig.6 Recovery strain of Ni-Mn-Cr-Ga alloys under different residual strains

## 4 Conclusions

1)  $\text{Ni}_{56}\text{Mn}_{25-x}\text{Cr}_x\text{Ga}_{19}$  ( $x=0, 2, 4, 6$ ) alloys exhibit single martensite phase for  $x=0$ , and dual-phase containing a tetragonal structured martensite and a face-centered cubic  $\gamma$  phase for  $x \geq 2$ . The amount of  $\gamma$  phase increases with increasing Cr content. The martensitic transformation temperature gradually decreases with increasing Cr content, which should be resulted from the variation in the intrinsic factors, i.e. the increase in the unit-cell volumes and the decrease in the electron concentration.

2) The improvement of ductility of  $\text{Ni}_{56}\text{Mn}_{25-x}\text{Cr}_x\text{Ga}_{19}$  alloys has been achieved by Cr addition. When  $x=4$ , the volume fraction of  $\gamma$  phase is

16%, the tensile stress and strain are 497 MPa and 8% for  $\text{Ni}_{56}\text{Mn}_{21}\text{Cr}_4\text{Ga}_{19}$  alloy, respectively.

3) The shape memory effects of  $\text{Ni}_{56}\text{Mn}_{25-x}\text{Cr}_x\text{Ga}_{19}$  ( $x=4, 6$ ) alloys increase gradually with increasing pre-strains. The recovery strain is 2.7% under a residual strain of 4.5% for  $\text{Ni}_{56}\text{Mn}_{21}\text{Cr}_4\text{Ga}_{19}$  alloy; and this value is 1.9% under a residual strain of 3.5% for  $\text{Ni}_{56}\text{Mn}_{19}\text{Cr}_6\text{Ga}_{19}$  alloy.

## References

- [1] ULLAKKO K, HUANG J K, KANTNER C, O'HANDLEY R C, KOKORIN V V. Large magnetic-field-induced strains in  $\text{Ni}_2\text{MnGa}$  single crystals [J]. Applied Physics Letters, 1996, 69(13): 1966–1968.
- [2] SOZINOV A, LIKHACHEV A, LANSKA N, ULLAKKO K. Giant magnetic-field-induced strain in NiMnGa seven-layered martensitic phase [J]. Applied Physics Letters, 2002, 80(10): 1746–1748.
- [3] MURRAY S J, MARIONI M, ALLEN S M, O'HANDLEY R C, LOGRASSO T A. 6% magnetic-field-induced strain by twin-boundary motion in ferromagnetic Ni-Mn-Ga [J]. Applied Physics Letters, 2000, 77(6): 886–888.
- [4] JING X, MARIONI M, BONO D, ALLEN S M, O'HANDLEY R C, HSU T Y. Empirical mapping of Ni-Mn-Ga properties with composition and valence electron concentration [J]. Journal of Applied Physics, 2002, 91(10): 8222–8224.
- [5] JIANG Cheng-bao, FENG Gen, GONG Sheng-kai, XU Hui-bin. Effect of Ni excess on phase transformation temperatures of NiMnGa alloys [J]. Materials Science and Engineering A, 2003, 342: 231–235.
- [6] MA Yun-qing, JIANG Cheng-bao, FENG Gen, XU Hui-bin. Thermal stability of the  $\text{Ni}_{54}\text{Mn}_{25}\text{Ga}_{21}$  Heusler alloy with high temperature transformation [J]. Scripta Materialia, 2003, 48(4): 365–369.
- [7] MA Yun-qing, JIANG Cheng-bao, LI Yan, XU Hui-bin, WANG Cui-ping, LIU Xing-jun. Microstructure and high-temperature shape-memory effect in  $\text{Ni}_{54}\text{Mn}_{25}\text{Ga}_{21}$  alloy [J]. Transactions of Nonferrous Metals Society of China, 2006, 16(3): 502–506.
- [8] XU Hui-bin, MA Yun-qing, JIANG Cheng-bao. A high-temperature shape-memory alloy  $\text{Ni}_{54}\text{Mn}_{25}\text{Ga}_{21}$  [J]. Applied Physics Letters, 2003, 82(19): 3206–3208.
- [9] ONO N, TSUKAHARA A, KAINUMA R, ISHIDA K. Properties of two-phase Ni-Al-Fe shape memory alloys in the virgin and shape-memory-cycled states [J]. Materials Science and Engineering A, 1998, 273: 420–424.
- [10] TANAKA Y, OIKAWA K, SUTOU Y, OMORI T, KAINUMA R, ISHIDA K. Martensitic transition and superelasticity of Co-Ni-Al ferromagnetic shape memory alloys with  $\beta+\gamma$  two-phase structure [J]. Materials Science and Engineering A, 2006, 438: 1054–1060.
- [11] XIN Yan, LI Yan, CHAI Liang, XU Hui-bin. Shape memory characteristics of dual-phase Ni-Mn-Ga based high temperature shape memory alloys [J]. Scripta Materialia, 2007, 57(7): 599–601.
- [12] DONG G F, CAI W, GAO Z Y, SUI J H. Effect of isothermal ageing on microstructure, martensitic transformation and mechanical properties of  $\text{Ni}_{53}\text{Mn}_{23.5}\text{Ga}_{18.5}\text{Ti}_5$  ferromagnetic shape memory alloy [J]. Scripta Materialia, 2008, 58(8): 647–650.
- [13] TSUCHIYA K, TSUTSUMI A, OHTSUKA H, UMEMOTO M. Modification of Ni-Mn-Ga ferromagnetic shape memory alloy by addition of rare earth elements [J]. Materials Science and Engineering A, 2004, 378(1–2): 370–376.
- [14] MA Yun-qing, YANG Shui-yuan, LIU Yong, LIU Xing-jun. The ductility and shape-memory properties of Ni-Mn-Co-Ga high-temperature shape-memory alloys [J]. Acta Materialia, 2009, 57(11):

- 3232–3241.
- [15] MA Yun-qing, JIANG Cheng-bao, LI Yan, XU Hui-bin, WANG Cui-ping, LIU Xing-jun. Study of  $\text{Ni}_{50+x}\text{Mn}_{25}\text{Ga}_{25-x}$  ( $x=2-11$ ) as high-temperature shape-memory alloys [J]. Acta Materialia, 2007, 55(5): 1533–1541.
- [16] SÁNCHEZ-ALARCOS V, PÉREZ-LANDEZÁBAL J I, RECARTE V, GÓMEZ-POLO C, RODRÍGUEZ-VELAMAZÁN J A. Correlation between composition and phase transformation temperatures in Ni-Mn-Ga-Co ferromagnetic shape memory alloys [J]. Acta Materialia, 2008, 56(19): 5370–5376.
- [17] CHEN X Q, LU X, WANG DY, QIN Z X. The effect of Co-doping on martensitic transformation temperatures in Ni-Mn-Ga Heusler alloys [J]. Smart Materials and Structures, 2008, 17: 065030.
- [18] CONG D Y, WANG S, WANG Y D, REN Y, ZUO L, ESLING C. Martensitic and magnetic transformation in Ni-Mn-Ga-Co ferromagnetic shape memory alloys [J]. Materials Science and Engineering A, 2008, 473(1–2): 213–218.
- [19] MA Yun-qing, YANG Shui-yuan, JIN Wan-jun, LIU Xing-jun.  $\text{Ni}_{56}\text{Mn}_{25-x}\text{Cu}_x\text{Ga}_{19}$  ( $x=0, 1, 2, 4, 8$ ) high-temperature shape-memory alloys [J]. Journal of Alloys and Compounds, 2009, 471(1–2): 570–574.

## $\text{Ni}_{56}\text{Mn}_{25-x}\text{Cr}_x\text{Ga}_{19}$ ( $x=0, 2, 4, 6$ ) 高温形状记忆合金

马云庆, 赖三哩, 杨水源, 罗渝, 王翠萍, 刘兴军

厦门大学 材料学院, 厦门 361005

**摘要:** 详细地研究了  $\text{Ni}_{56}\text{Mn}_{25-x}\text{Cr}_x\text{Ga}_{19}$  ( $x=0, 2, 4, 6$ ) 合金的微观组织结构、马氏体相变特性、力学性能及形状记忆效应。结果表明: 当  $x=0$  时, 合金呈现出单一的四方结构马氏体相; 当  $x \geq 2$  时, 合金的微观组织为包含马氏体相和  $\gamma$  相的双相结构; 随着 Cr 元素的增加, 合金的马氏体相变温度逐渐降低, 其峰值温度从  $x=0$  时的  $401\text{ }^\circ\text{C}$  降低到  $x=6$  时的  $197\text{ }^\circ\text{C}$ 。热轧和拉伸试验表明: 通过添加 Cr 元素在合金微观组织中引入  $\gamma$  相可有效地提高合金的热加工性能和塑性,  $x \geq 4$  的合金可通过常规热轧得到表面状态良好的  $1\text{ mm}$  厚的片材, 合金的拉伸应力和应变在  $x=4$  和  $6$  时分别为  $497\text{ MPa}$ ,  $8\%$  和  $454\text{ MPa}$ ,  $5.5\%$ ;  $x=4$  的合金在残余应变为  $4.5\%$  时可得到  $2.7\%$  的形状记忆回复, 而  $x=6$  的合金在残余应变为  $3.5\%$  时的可回复应变为  $1.9\%$ 。

**关键词:** 马氏体相变; 拉伸; 韧性; 高温形状记忆效应

(Edited by YANG Hua)